The nonlinear evolution of unstable coupled equatorial ocean-atmosphere modes

P. C. F. van Der Vaart, H. A. Dijkstra

Nonlinear Processes in Geophysics (1998) 5: 39–52

Nonlinear Processes in Geophysics

The nonlinear evolution of unstable coupled equatorial ocean-atmosphere modes

P. C. F. van der Vaart and H. A. Dijkstra

Institute for Marine and Atmospheric Research Utrecht, Utrecht University, The Netherlands

Received: 30 June 1997 – Accepted: 1 June 1998

Abstract. In this paper we investigate whether observed intraseasonal variability in the equatorial Pacific can be attributed to finite amplitude waves resulting from unstable air-sea interactions. Within a Zebiak - Cane type model of the coupled equatorial ocean - atmosphere, the nonlinear equilibration of instabilities of a simple basic state is considered with periodic conditions on the ocean boundaries. Three mechanisms exist which can induce a finite amplitude equilibration on a time scale $\epsilon^2 t$. Here t is the characteristic time scale of growth of the disturbance and ϵ the relative distance from the instability threshold. For each equilibration mechanism, the finite amplitude and period of the equilibrium state are computed as a function of ϵ and substantial amplitude can be reached for a reasonable degree of supercriticality. Thereafter the analysis is extended to include time-dependent external forcing. It is shown that interannual variability may result through the interaction of the response of a weak annual external forcing and the finite amplitude development of the intraseasonal instabilities.

1 Introduction

The equatorial ocean-atmosphere system is a strongly coupled dynamical system displaying spatio-temporal variability on a number of scales. One of the important origins of this variability is the existence of coupled feedbacks between the ocean and atmosphere (Bjerknes, 1969). Apart from the much studied El-Nino/Southern Oscillation phenomenon (Philander, 1990), there is considerable variability in the Pacific Ocean on intraseasonal time scales.

In earlier studies (Enfield, 1987; Spillane et al., 1987) it has been suggested that intraseasonal variations in sea level along the west coast of the Americas is remotely forced by atmospheric variability in the western Pacific. Further analysis of temperature, wind and current observations (Johnson and McPhaden, 1993; McPhaden and Taft, 1988) showed intraseasonal variability in subsurface temperature and zonal current which could be well described in terms of propagating (first baroclinic) Kelvin type modes. The discrepancies between the observed spatial pattern and that of the free equatorial oceanic Kelvin mode were attributed to wave/-mean flow interaction. No local coherence between subsurface anomalies and wind stress anomalies was found (Johnson and McPhaden, 1993), but in a recent study Kessler and Weickmann (1995) demonstrated a non-local coherence between windstress and sea surface temperature (SST) anomalies.

They proposed that ocean-atmosphere coupling is involved in the forcing and maintenance of the Kelvin modes.

It has been known for some time that positive feedbacks in the equatorial ocean atmosphere system may cause strong amplification of small disturbances which may, when grown to finite amplitude, modify the evolution of the seasonal cycle or spatial structure of the annual mean state. The instabilities of a simplified annual mean state have been well identified in intermediate coupled ocean/atmosphere models. One of the models which is believed to capture most of the essential physics of the coupled system is that of Zebiak and Cane (1987), referred to below as the ZC-model. For a spatially constant climatology the most unstable traveling wave modes were determined by Hirst (1986) and Neelin (1991) in a ZC-model with periodic boundary conditions at the meridional ocean boundaries. The latter boundary conditions can be assumed in studies of intraseasonal variability since the reflection at the ocean boundaries is not important. Hirst (1986) focuses on two types of coupled long wavelength traveling waves which can become unstable under favorable conditions (i.e. strong coupling). Both classes are related to free ocean waves, i.e. long Rossby waves and Kelvin waves, and have corresponding frequencies. Although Hirst (1986) mentions that a third class of traveling waves – related to the evolution of the sea surface temperature (SST) – is possible, Neelin (1991) demonstrated the relevance of these SST modes for the variability of the equatorial system.

In Neelin (1991) the different classes of modes are nicely

Correspondence to: P. C. F. van der Vaart

classified with help of the coefficients in the linearized SST-equation, e.g. written as

$$\delta_{sst}\frac{\partial T}{\partial t} + \kappa_z u - \kappa_{Th} h + \kappa_u w + \kappa_d T = 0$$

where T, u, h and w are the SST, zonal advection, thermocline and vertical velocity anomaly, respectively. Furthermore, the subscripts z, Th, u and d in the coefficients κ refer to zonal advection feedback, thermocline feedback, upwelling feedback and damping, respectively. The coefficient δ_{sst} is the relative time scale of development of ocean waves to that of the SST anomalies. Using this equation, coupled Kelvin waves are preferred when $\kappa_z = \kappa_u = 0$, coupled Rossby waves when $\kappa_{Th} = \kappa_u = 0$ and SST-waves are possible whenever δ_{sst} is unequal to zero. Each mechanism of destabilization is directly related to the coefficients above, for example when the term $\kappa_{Th}h$ causes the destabilization the wave is said to become unstable through thermocline feedback. These basic results for the stability of zonally constant basic states in the periodic basin case have been extended in subsequent studies to include more detailed physics both of the atmosphere and the ocean. For example, in Hirst and Lau (1990) the effect of wave propagation in a moist atmosphere is considered. The Hirst (1986) modes may be strongly modified by the inclusion of more detailed physics in the atmosphere but the basic characteristics and destabilization mechanisms remain the same.

Although much is known about the linear stability of a number of different basic states, relatively little is known about the nonlinear evolution of the coupled traveling waves. The study of the equilibration of unstable coupled modes and their subsequent transitions is important to determine whether these modes can obtain sufficient amplitude to be related to the intraseasonal variability in the equatorial ocean-atmosphere system. The key to study this equilibration of the instabilities is model reduction through projection of the dynamical system on the dynamically active modes. In this paper, such a reduction technique for the periodic basin case is presented and applied to study the finite amplitude equilibration of the Hirst (1986) coupled instabilities. The focus of the study is on the method of reduction, which has a large application potential, and on the qualitative aspects of the results, rather than on a more detailed comparison with observations which will be presented elsewhere.

In section 2 the coupled model is shortly recalled and the methods of analysis are presented in quite some detail. Next the linear stability of a simple basic state and the weakly nonlinear equilibration of the instabilities is studied. The nonlinear evolution of the instabilities is shown to be governed by a complex Ginzburg-Landau equation of which we consider only the (stable) Stokes wave solution. The latter solution shows how nonlinearities balance the exponential growth of the instability which results in a finite amplitude bounded state.

Observations of the intraseasonal Kelvin modes also indicate a consistent low-frequency modulation and are therefore thought to be important in the initiation and sustain of ENSO events by affecting SST (Lau and Shen, 1988). In the last section, the reduction technique is extended to include an annual period weak external forcing in windstress. It is demonstrated that such a small amplitude windstress fluctuation may transfer energy to interannual frequencies during equilibration of the instabilities.

2 Formulation of the problem

2.1 Model

The intermediate model used in this study is similar to that used by Hirst (1986). The atmospheric component consists of a linear Gill model (Gill, 1980) forced by latent heat release proportional to sea surface temperature (SST) anomalies.

$$\begin{aligned} U_t + AU - \beta y V + P_x &= 0 \\ V_t + AV + \beta y U + P_y &= 0 \\ P_t + AP + c_a^2(U_x + V_y) &= -K_Q T \end{aligned} \qquad (1a)$$

where (U, V) are the horizontal velocities and P is the geopotential height, A is a damping coefficient and c_a the wave speed of the first baroclinic Kelvin wave. The ocean component is a 1.5 layer nonlinear reduced gravity model for the zonal and meridional velocities u and v and the thermocline depth h without the usual mixed layer as in the ZC- model, forced by wind stress anomalies proportional to the atmospheric surface winds. The governing equations are

$$\begin{aligned} u_t + ru - \beta y v + g' h_x + u u_x + v u_y &= \gamma_\tau U \\ v_t + rv + \beta y u + g' h_y + u v_x + v v_y &= \gamma_\tau V \\ h_t + rh + u_x + v_y + (uh)_x + (vh)_y &= 0 \end{aligned} \qquad (1b)$$

In the equations above, nonlinear ocean dynamics is taken into account because of its potential influence on the nonlinear development of the coupled modes, as is known for the uncoupled ocean case (Boyd, 1980a,b). The evolution of the SST anomalies T on a basic state (indicated by the barred quantities) with constant upwelling $\overline{w}$, constant thermocline depth $\overline{h} = H$ and constant zonal temperature gradient $\overline{T}_x$ is governed by

$$\delta_{sst} T_t + dT + \overline{T}_x u + \frac{\overline{w}}{H} T + \frac{1}{H}(\overline{T} - T_s(\overline{h}))w - \frac{\overline{w}}{H} T_s'(\overline{h}) h$$

$$+ \frac{1}{H} T w - \frac{T_s'(\overline{h})}{H} w h + u T_x + v T_y = 0 \qquad (1c)$$

where T_s is the (subsurface) temperature of water just below the thermocline assumed proportional to h, just as in Hirst (1986). The vertical velocity component w is obtained from the continuity equation and the constant d is a damping (Newtonian cooling) coefficient.

The boundary conditions for the ocean atmosphere coupled system are periodic in the zonal direction and all quantities are bounded in the meridional direction, i.e.

Table 1. Standard values of the dimensional parameters.

g'	$0.03\ m\ s^{-2}$
β	$2.23 \times 10^{-11}\ m^{-1}\ s^{-1}$
$\mathcal{T}_o$	$1.5 \times 10^5\ s$
$\mathcal{L}_o$	$2.50 \times 10^5\ m$
H	$150\ m$
c_o	$2.0\ m\ s^{-1}$
c_a	$30.0\ m\ s^{-1}$
r	$1.3 \times 10^{-6} s^{-1}$
A	$5.9 \times 10^{-6}\ s^{-1}$
d	$1.3 \times 10^{-6}\ s^{-1}$
$\overline{T}_x$	$-5.0 \times 10^{-7}\ K\ m^{-1}$
$\Delta\overline{T}$	$14\ K$
$\overline{h}$	$150\ m$
$\overline{w}$	$1.7 \times 10^{-5}\ m\ s^{-1}$
$\overline{T}$	$28\ K$
$T_s(\overline{h})$	$4\ K$
$T_s'(\overline{h})$	$0.03\ K\ m^{-1}$
k_Q	$7.0 \times 10^{-3}\ m^2\ s^{-3}\ K^{-1}$

$$\left(\begin{array}{cccccc} u & v & h & T & U & V & \phi \end{array} \right)^T \rightarrow 0 \quad , \quad |y| \rightarrow \infty \tag{1d}$$

The coupled system is nondimensionalized using the time scale $\mathcal{T}_o$ and lengthscale $\mathcal{L}_o$ defined as

$$\mathcal{T}_o = \sqrt{\frac{1}{\beta c_o}} \quad , \quad \mathcal{L}_o = \sqrt{\frac{c_o}{\beta}}$$

where c_0, the characteristic phase speed of an oceanic Kelvin wave,

$$c_o = \sqrt{g'H},$$

is the horizontal velocity scale. The thermocline depth is scaled with H and the sea surface temperature by a characteristic temperature difference ΔT. In the atmosphere, the geopotential height and the horizontal velocities are nondimensionalized by c_a^2 and $c_o \frac{K_Q \Delta T \mathcal{T}_o}{c_a^2}$, respectively. Using these scales, the dimensionless parameters in the system are

$$\epsilon_o = \mathcal{T}_o r \qquad \epsilon_a = \mathcal{T}_o A \qquad \kappa_d = \mathcal{T}_o d$$

$$c = \frac{c_a}{c_o} \qquad \kappa_z = \frac{\overline{T}_x \mathcal{L}_o}{\Delta T} \qquad \mu = \gamma_\tau K_Q \Delta T \mathcal{T}_o^2 / c_o^2$$

$$\kappa_{Th} = \frac{T_s'(\overline{h}) H}{\Delta T} \qquad \kappa_u = \frac{\overline{T} - T_s(\overline{h})}{\Delta T} \qquad \kappa_w = \frac{\overline{w} \mathcal{T}_o}{H}$$

Estimates of the dimensional quantities obtained for the basic state are based on Hirst (1986) and given in Table 1.

The dimensionless SST equation becomes

$$(\delta_{sst}\partial_t + \kappa_w + \kappa_d)T + \kappa_z u + \kappa_u w$$

Table 2. Standard values of dimensionless parameters in the model.

ϵ_o	0.2	ϵ_a	0.9
κ_d	0.42	c	15.0
κ_z	$-1.0\ 10^{-2}$	κ_{Th}	0.21
κ_w	0.02	κ_u	1.71

$$-\kappa_w \kappa_{Th} h + u T_x + v T_y + (T - \kappa_{Th} h) w = 0$$

in which the governing processes can be identified by its dimensionless parameters. For example, κ_z represents the strength of zonal advection, the term $\kappa_w \kappa_{Th} h$ controls the effect of thermocline feedback, κ_u the upwelling feedback and $\kappa_w + \kappa_d$ is the damping coefficient. Standard values for these parameters are given in Table 2.

The nondimensional system of equations can be written into the general form

$$\begin{cases} (\mathcal{M}\frac{\partial}{\partial t} + \mathcal{L})\mathbf{\Phi} + \mathcal{N}(\mathbf{\Phi})\mathbf{\Phi} = \mathbf{0} \\ \mathcal{B}(\mathbf{\Phi}) = \mathbf{0} \end{cases} \tag{2}$$

where the operator $\mathcal{B}$ specifies the boundary conditions. For the specific problem, $\mathbf{\Phi}$ is given by

$$\mathbf{\Phi} = \left(\begin{array}{ccccccc} u & v & h & T & U & V & P \end{array} \right)^T \tag{3a}$$

and the linear operators $\mathcal{M}$, $\mathcal{L}$ are defined as

$$\mathcal{M} = diag(\ 1, 1, 1, \delta_{sst}, 1, 1, 1\ ) \tag{3b}$$

$$\mathcal{L} = \begin{pmatrix} \epsilon_o & -y & \partial_x & 0 & -\mu & 0 & 0 \\ y & \epsilon_o & \partial_y & 0 & 0 & -\mu & 0 \\ \partial_x & \partial_y & \epsilon_o & 0 & 0 & 0 & 0 \\ \kappa_z + \kappa_u \partial_x & \kappa_u \partial_y & -\kappa_w \kappa_{Th} & \kappa_d + \kappa_w & 0 & 0 & 0 \\ 0 & 0 & 0 & 0 & \epsilon_a & -y & \partial_x \\ 0 & 0 & 0 & 0 & y & \epsilon_a & \partial_y \\ 0 & 0 & 0 & 1 & c^2\partial_x & c^2\partial_y & \epsilon_a \end{pmatrix} \tag{3c}$$

and the nonlinear operator $\mathcal{N}(\mathbf{\Phi})$, given by

$$\mathcal{N}(\mathbf{\Phi}) = \begin{pmatrix} u\partial_x + v\partial_y & 0 & 0 & 0 & 0 & 0 & 0 \\ 0 & u\partial_x + v\partial_y & 0 & 0 & 0 & 0 & 0 \\ h\partial_x & h\partial_y & u\partial_x + v\partial_y & 0 & 0 & 0 & 0 \\ T\partial_x + T_x & T\partial_y + T_y & -\kappa_{Th} w & 0 & 0 & 0 & 0 \\ 0 & 0 & 0 & 0 & 0 & 0 & 0 \\ 0 & 0 & 0 & 0 & 0 & 0 & 0 \\ 0 & 0 & 0 & 0 & 0 & 0 & 0 \end{pmatrix} \tag{3d}$$

with $w = \partial_x u + \partial_y v$, contains the quadratic nonlinear interactions.

Three different types of nonlinearity will be compared with respect to the finite amplitude equilibration and phase modulation that they generate. First only nonlinear upwelling feedback will be taken into account (case A), i.e. advection of perturbations is absent in both ocean and SST equations. This type of nonlinearity is found, for instance, in Wakata

and Sarachik (1994) to be the dominant equilibration mechanism. The second case (B) includes advection of SST perturbations, as it is taken into account in intermediate models of ZC-type. In case C, nonlinear ocean dynamics is also active in addition to the other two equilibration mechanisms.

2.2 Linear stability analysis

A linear stability analysis is the basis of any weakly nonlinear analysis. Within this analysis sufficient conditions for instability are determined by considering the evolution of infinitesimally small perturbations $\mathbf{\Phi}$ in (2). For these perturbations, nonlinear terms can be neglected and the equations (2) reduce to

$$\begin{cases} (\mathcal{M}\frac{\partial}{\partial t} + \mathcal{L})\mathbf{\Phi} = \mathbf{0} \\ \mathcal{B}(\mathbf{\Phi}) = \mathbf{0} \end{cases} \tag{4}$$

The geometry allows for traveling wave solutions in the x - direction with wavenumber k and complex growth factor σ, i.e.

$$\mathbf{\Phi}(x,y,t) = \hat{\mathbf{\Phi}}(y)e^{ikx+\sigma t} + c.c.$$

where $c.c.$ indicates complex conjugate. On substitution into (4) we obtain the two-point boundary value problem for the eigenpair $(\sigma, \hat{\mathbf{\Phi}})$,

$$\begin{cases} (\hat{\mathcal{M}}(k)\,\sigma + \hat{\mathcal{L}}(k))\hat{\mathbf{\Phi}} = \mathbf{0} \\ \hat{\mathbf{\Phi}}(y = \pm\infty) = \mathbf{0} \end{cases} \tag{5}$$

where the operators $\hat{\mathcal{M}}(k)$ and $\hat{\mathcal{L}}(k)$ are the Fourier transforms of $\mathcal{M}$ and $\mathcal{L}$ in the x - direction. For the stability problem of the model under consideration, the operators $\hat{\mathcal{M}}(k)$ and $\hat{\mathcal{L}}(k)$ are given by

$$\hat{\mathcal{M}}(k) = \mathcal{M}$$

$$\hat{\mathcal{L}} = \begin{pmatrix} \epsilon_o & -y & ik & 0 & -\mu & 0 & 0 \\ y & \epsilon_o & \partial_y & 0 & 0 & -\mu & 0 \\ ik & \partial_y & \epsilon_o & 0 & 0 & 0 & 0 \\ \kappa_z + ik\kappa_u & ik\kappa_u & -\kappa_w\kappa_{Th} & \kappa_d+\kappa_w & 0 & 0 & 0 \\ 0 & 0 & 0 & 0 & \epsilon_a & -y & ik \\ 0 & 0 & 0 & 0 & y & \epsilon_a & \partial_y \\ 0 & 0 & 0 & 1 & ikc^2 & c^2\partial_y & \epsilon_a \end{pmatrix}$$

The eigenvalue σ is written as $\sigma = \lambda + i\omega$ and considered as a function of the wavenumber k and a control parameter μ; the latter can be any parameter in the system. The real part λ determines the stability of the basic state with respect to the small perturbations. If $\lambda > 0$ these grow exponentially and the basic state is unstable. The neutral curve, $\lambda(k,\mu) = 0$ in the (k,μ) plane provides sufficient conditions for instability. In many applications, the neutral curve has a minimum at (k_c, μ_c), at which

$$\lambda(k_c,\mu_c) = 0\ ,\ \frac{\partial\lambda}{\partial k}(k_c,\mu_c) = 0\ ,\ \frac{\partial^2\lambda}{\partial k^2}(k_c,\mu_c) < 0 \tag{6}$$

Physically, k_c is the wavenumber of the first wave to become unstable as μ is increased beyond μ_c.

2.3 Weakly nonlinear analysis

The linear theory shows that, under conditions (6) and if μ is larger than μ_c, wavelike perturbations exist with exponentially growing amplitudes. This description is only valid in the initial growth stage, where the wave amplitudes are infinitesimally small. To describe their evolution to finite amplitude, the nonlinear interactions between the various wave components must be taken into account. Further analysis is possible if the control parameter μ is considered slightly above its critical value μ_c, i.e.

$$\mu = \mu_c + m\epsilon^2 \tag{7a}$$

where

$$\epsilon \ll 1\ ,\ \ m = \mathcal{O}(1) \tag{7b}$$

The approximation of the neutral curve by a parabola near its minimum, then implies that

$$|k - k_c| = \mathcal{O}(\epsilon). \tag{7c}$$

The unstable waves are thus limited to a narrow band around the critical wavenumber k_c and this band can be interpreted as a wavepacket, with central wavenumber k_c. This wavepacket evolves on a time scale which is large compared to the typical wave periods and is characterized by scales

$$T = \epsilon^2 t\ ,\ X = \epsilon(x - c_g t) \tag{7d}$$

where c_g is the group velocity, which is determined by the dispersion relation at criticality. The long spatial scale X is a slow moving coordinate, traveling with the group velocity of the unstable wavepacket. This scaling leads to the transformations

$$\frac{\partial}{\partial t} \to \frac{\partial}{\partial t} - \epsilon c_g\frac{\partial}{\partial X} + \epsilon^2\frac{\partial}{\partial T}\ ,\ \ \frac{\partial}{\partial x} \to \frac{\partial}{\partial x} + \epsilon\frac{\partial}{\partial X} \tag{7e}$$

The finite amplitude of the perturbations will be small compared to that of the basic state, for μ close to μ_c, so the solution vector $\mathbf{\Phi}$ is expanded Newell and Whitehead (1969) in terms of the small parameter ϵ and Fourier modes of the marginally stable wave $E = exp(i[k_c x + \omega_c t])$, i.e.

$$\mathbf{\Phi} = \begin{array}{ccc} \epsilon\mathbf{\Phi}^{(11)}E & & +\cdots \\ +\epsilon^2(\mathbf{\Phi}^{(02)} & +\mathbf{\Phi}^{(12)}E & +\mathbf{\Phi}^{(22)}E^2 + \cdots) \\ + & \epsilon^3\mathbf{\Phi}^{(13)}E & +\cdots + c.c. \end{array} \tag{8}$$

where $\mathbf{\Phi} = \mathbf{\Phi}(x,X,y,t,T)$ and $\mathbf{\Phi}^{(ij)} = \mathbf{\Phi}^{(ij)}(X,y,T)$. In the expansion (8), only the terms relevant to obtain the final reduced model are taken into account. By substitution of the expansions (8) into (2) and collecting terms of like orders in ϵ and E one can reduce the full equations to a scalar equation for the envelope of the most unstable wave packet. Because some of the steps within the analysis have interesting physical interpretations, and the analysis is applicable to a large class of stability problems, we present it here in more detail.

At $\mathcal{O}(\epsilon E)$ the linear stability problem (5) is recovered

$$(i\omega_c\hat{\mathcal{M}}(k) + \hat{\mathcal{L}}(k))\mathbf{\Phi}^{(11)} = 0 \tag{9a}$$

The equations at $\mathcal{O}(\epsilon^2 E)$,

$$(i\omega_c\hat{\mathcal{M}}(k_c)+\hat{\mathcal{L}}(k_c))\mathbf{\Phi}^{(12)} =$$

$$-(\hat{\mathcal{L}}_k(k_c)+i\omega_c\hat{\mathcal{M}}_k(k_c)-c_g\hat{\mathcal{M}}(k_c))\frac{\partial\mathbf{\Phi}^{(11)}}{\partial X}, \qquad (9b)$$

where a subscript indicates differentiation of the operator with respect to the indicated parameter, can only have a solution, if the righthand side satisfies a Fredholm orthogonality condition. This solution is non-unique, for we can add the solution of the homogeneous problem. The latter will be omitted here since it does not play a role in the derivation of final amplitude equation.

At $\mathcal{O}(\epsilon^2)$ and at $\mathcal{O}(\epsilon^2 E^2)$ two invertible problems describe the nonlinear self-interaction of the marginally stable wave. This results in a modification of the basic state and a second harmonic contribution given by $\mathbf{\Phi}^{(02)}$ and $\mathbf{\Phi}^{(22)}$, respectively, which satisfy

$$\hat{\mathcal{L}}(0)\mathbf{\Phi}^{(02)} = -2Re(\mathcal{N}(\mathbf{\Phi}^{(11)})\mathbf{\Phi}^{(11)\,*} \qquad (9c)$$

$$(2i\omega_c\hat{\mathcal{M}}(2ik_c)+\hat{\mathcal{L}}(2ik_c))\mathbf{\Phi}^{(22)} = -\mathcal{N}(\mathbf{\Phi}^{(11)})\mathbf{\Phi}^{(11)} \qquad (9d)$$

where Re indicates real part and $*$ the complex conjugate. Since the linear operator $i\omega_c\hat{\mathcal{M}}+\hat{\mathcal{L}}$ does not act on the long scales X and T, the eigenvector $\mathbf{\Phi}^{(11)}$ is written as $A(X,T)\mathbf{\Psi}$. Substitution of this expression into the equations at higher order leads to the following dependencies on the amplitude A.

$$\mathbf{\Phi}^{(11)} = A(X,T)\mathbf{\Psi}(y)$$

$$\mathbf{\Phi}^{(12)} = \frac{\partial A}{\partial X}(X,T)\mathbf{\Psi}^{(12)}(y)$$

$$\mathbf{\Phi}^{(02)} = |A(X,T)|^2\mathbf{\Psi}^{(02)}(y)$$

$$\mathbf{\Phi}^{(22)} = A^2(X,T)\mathbf{\Psi}^{(22)}(y)$$

The vectors $\mathbf{\Psi}^{(12)}$, $\mathbf{\Psi}^{(02)}$ and $\mathbf{\Psi}^{(22)}$ satisfy

$$(i\omega_c\hat{\mathcal{M}}(k_c)+\hat{\mathcal{L}}(k_c))\mathbf{\Psi}^{(12)} =$$

$$-(\hat{\mathcal{L}}_k(k_c)+i\omega_c\hat{\mathcal{M}}_k(k_c)-c_g\hat{\mathcal{M}}(k_c))\mathbf{\Psi} \qquad (10a)$$

$$\hat{\mathcal{L}}(0)\mathbf{\Psi}^{(02)} = -2Re(\mathcal{N}(\mathbf{\Psi})\mathbf{\Psi}^*) \qquad (10b)$$

$$(2i\omega_c\hat{\mathcal{M}}(2ik_c)+\hat{\mathcal{L}}(2ik_c))\mathbf{\Psi}^{(22)} = -\mathcal{N}(\mathbf{\Psi})\mathbf{\Psi} \qquad (10c)$$

and these equations are complemented with the appropriate boundary conditions at this order in the expansion. The group velocity of the unstable wave packet appears as the Fredholm solvability condition in the righthand side of the singular problem (10b). From differentiation of the eigenvalue problem and inspection of the right hand side of equation (10a) it is observed that the solution $\mathbf{\Psi}^{(12)}$ and the group velocity are given by

$$\mathbf{\Psi}^{(12)} = -i\frac{\partial\mathbf{\Psi}}{\partial k} \;\;,\;\; c_g = \frac{\partial\omega}{\partial k} \qquad (11)$$

both evaluated at criticality. The equations (10b) and (10c) are regular and can be solved directly for $\mathbf{\Psi}^{(02)}$ and $\mathbf{\Psi}^{(22)}$.

At $\mathcal{O}(\epsilon^3 E)$ a singular problem is obtained for which the right-hand side now depends explicitly on the amplitude $A(X,T)$ and the vectors $\mathbf{\Psi}$, $\mathbf{\Psi}^{(12)}$, $\mathbf{\Psi}^{(02)}$ and $\mathbf{\Psi}^{(22)}$, i.e.

$$(i\omega_c\hat{\mathcal{M}}(k_c)+\hat{\mathcal{L}}(k_c))\mathbf{\Phi}^{(13)} =$$

$$-(\hat{\mathcal{M}}(k_c)\mathbf{\Psi}\,\frac{\partial A}{\partial T}+m\mathbf{\Gamma}A+\frac{1}{2}\mathbf{\Sigma}\,\frac{\partial^2 A}{\partial X^2}+\mathbf{\Lambda}\,A|A|^2) \qquad (12)$$

where

$$\mathbf{\Gamma} = (\hat{\mathcal{L}}_\mu(k_c)-i\omega_c\hat{\mathcal{M}}_\mu(k_c))\mathbf{\Psi}, \qquad (13a)$$

$$\mathbf{\Sigma} = (i\omega_c\hat{\mathcal{M}}_{kk}(k_c)-\hat{\mathcal{L}}_{kk}(k_c)-2c_g\hat{\mathcal{M}}_k(k_c))\mathbf{\Psi}$$

$$+2i(i\omega_c\hat{\mathcal{M}}_k(k_c)-c_g\hat{\mathcal{M}}(k_c)-\hat{\mathcal{L}}_k(k_c))\mathbf{\Psi}_k \qquad (13b)$$

and the vector $\mathbf{\Lambda}$ contains all nonlinear interactions at this order

$$\mathbf{\Lambda} = \mathcal{N}(\mathbf{\Psi})\mathbf{\Psi}^{(02)}+\mathcal{N}(\mathbf{\Psi}^{(02)})\mathbf{\Psi}$$
$$+\mathcal{N}(\mathbf{\Psi}^{(22)})\mathbf{\Psi}^*+\mathcal{N}(\mathbf{\Psi}^*)\mathbf{\Psi}^{(22)} \qquad (13c)$$

In general, the right hand side of (12) is not contained in the range of $i\omega_c\hat{\mathcal{G}}+\hat{\mathcal{L}}$. Valid solutions to (12), on an $\mathcal{O}(1/\epsilon^2)$ time scale, are possible if the right-hand side is orthogonal to the kernel of the linear operator in the left-hand side. This so called solvability condition is a direct result of the Fredholm alternative. Since the kernel of this operator has dimension 1, it is spanned by 1 vector, say $\mathbf{Q}$, which implies that $\mathbf{Q}^H(i\omega_c\hat{\mathcal{G}}+\hat{\mathcal{L}})\mathbf{W} = 0$ under the appropriate innerproduct, where $\mathbf{W}$ is an arbitrary vector and H indicates Hermitian transposed.

The amplitude equation resulting from the solvability condition for (12) is called the Ginzburg-Landau equation :

$$\frac{\partial A}{\partial T} = \gamma_1 A+\gamma_2\frac{\partial^2 A}{\partial X^2}-\gamma_3 A|A|^2 \qquad (14a)$$

where the three coefficients in (14a), all evaluated at criticality ($k=k_c, \mu=\mu_c$) are given by

$$\gamma_1 = m\frac{\mathbf{Q}^H\mathbf{\Gamma}}{\mathbf{Q}^H\hat{\mathcal{M}}\mathbf{\Psi}} = m\frac{\partial\sigma}{\partial\mu} \qquad (14b)$$

$$\gamma_2 = \frac{\mathbf{Q}^H\mathbf{\Sigma}}{\mathbf{Q}^H\hat{\mathcal{M}}\mathbf{\Psi}} = -\frac{1}{2}\frac{\partial^2\sigma}{\partial k^2} \qquad (14c)$$

$$\gamma_3 = -\frac{\mathbf{Q}^H\mathbf{\Lambda}}{\mathbf{Q}^H\hat{\mathcal{M}}\mathbf{\Psi}} = -(\Lambda_r+i\Lambda_i) \qquad (14d)$$

It should be noted that the theory above is applicable if, in addition to (6), the modes at $k=0$ and $k=2\,k_c$ are damped at criticality. This condition validates the expansion (8) and has to be verified as part of the linear stability analysis. In case of a supercritical Hopf-bifurcation, i.e. $Re(\sigma_{mu})>0$, non- trivial bounded solutions to (14a) exist, if the coefficient

γ_3 has a positive real part. If these conditions are satisfied, (14a) can be rescaled into a standard form for analysis, by introducing new time, space and amplitude variables

$$\tau = \rho T \ , \ \xi = \eta X \ ; \ a(\xi,\tau) = a_\infty^{-1} A(X,T) e^{-im\omega_\mu T} \tag{15a}$$

The quantities ρ, η and a_∞ are given by

$$\rho = m\lambda_\mu \ ; \ \eta = \sqrt{-\frac{2m\lambda_\mu}{\lambda_{kk}}} \ ; \ a_\infty = \sqrt{-m\frac{\lambda_\mu}{\Lambda_r}} \tag{15b}$$

and again a subscript indicates differentiation, i.e. $\lambda_\mu = \frac{\partial \lambda}{\partial \mu}$. Finally, the standard Ginzburg-Landau equation

$$\frac{\partial a}{\partial \tau} = a + (1+i\alpha_1)\frac{\partial^2 a}{\partial \xi^2} - (1+i\alpha_2)\, a|a|^2 \tag{16a}$$

is obtained where the two coefficients (α_1, α_2) which determine the properties of the finite amplitude evolution of the wavepacket are given by

$$\alpha_1 = \frac{\omega_{kk}}{\lambda_{kk}} \quad ; \quad \alpha_2 = \frac{\Lambda_i}{\Lambda_r}, \tag{16b}$$

Im indicating imaginary part.

When a characteristic dimensionless time scale τ_0, a dimensionless length scale ξ_0 and an amplitude a_0 are found in the computed trajectories of solutions to (16a), these translate to physical quantities according to

$$(a_\infty^*)^2 = (\mu - \mu_c)\frac{-\lambda_\mu}{\Lambda_r} a_0^2 \tag{16c}$$

$$t_0^* = \mathcal{T}_o \frac{\tau_0}{(\mu - \mu_c)\lambda_\mu} \tag{16d}$$

$$x_0^* = \mathcal{L}_o \xi_0 \left(\frac{-\lambda_{kk}}{2(\mu-\mu_c)\lambda_\mu}\right)^{1/2} \tag{16e}$$

2.4 Numerical implementation

To reduce the boundary value problem associated with the linear stability analysis to an algebraic problem a pseudo-spectral method is used. The solutions are expanded in Rational Chebychev polynomials (Boyd, 1987)

$$TB_n(y) = cos\,[n(arccot(y/L))] \tag{17}$$

Expanding the eigenfunctions of the linear stability problem into a sum of the basisfunctions (17) up to order N and applying the two-point eigenvalue problem at the collocation points leads to a generalized $7N$-dimensional eigenvalue problem of the form

$$(\hat{\mathbf{G}}\,\sigma + \hat{\mathbf{L}})\hat{\mathbf{\Psi}} = \mathbf{0} \tag{18}$$

where the eigenvalue σ is a function of, among other parameters, k and μ. In the derivation of amplitude equations the critical point plays a central role as was seen above. It is important to determine this critical point with high accuracy, since the coefficients in the Ginzburg-Landau equation are evaluated at this point. Writing $\chi = (k, \mu)$ for notational convenience and λ is the real part of the eigenvalue σ , a function $\mathbf{F}$ is defined as,

$$\mathbf{F}(\chi) = \begin{pmatrix} \lambda(\chi) \\ \frac{\partial \lambda}{\partial k}(\chi) \end{pmatrix} = \mathbf{0} \tag{19a}$$

Applying the Newton-Raphson method to determine solutions of this system of nonlinear algebraic equations gives

$$\chi_{l+1} = \chi_l - (\mathbf{DF})^{-1}(\chi_l)\mathbf{F}(\chi_l) \tag{19b}$$

The Jacobian $\mathbf{DF}$ is given by

$$\mathbf{DF}(\chi) = \begin{pmatrix} \frac{\partial \lambda}{\partial k}(\chi) & \frac{\partial \lambda}{\partial \mu}(\chi) \\ \\ \frac{\partial^2 \lambda}{\partial k^2}(\chi) & \frac{\partial^2 \lambda}{\partial k \partial \mu}(\chi) \end{pmatrix} \tag{19c}$$

The components in (19c) are accurately and efficiently calculated from the generalized eigenvalue problem (18) and details are given in the appendix. If the Newton process has converged, the critical point (k_c, μ_c) is obtained and simultaneously the critical frequency ω_c, the groupvelocity c_g and the coefficients γ_1 and γ_2 in the Ginzburg-Landau equation.

A crucial step in the weakly nonlinear analysis is the application of the Fredholm alternative to the singular not self-adjoint system (12). Following Chen and Joseph (1990) and Newell et al. (1990), the vector $\mathbf{Q}$ in (14b-d) is obtained from the singular value decomposition of the discretized linear operator in the left hand side of (12), i.e.

$$i\omega_c \hat{\mathbf{G}} + \hat{\mathbf{L}} = \mathbf{W}\mathbf{S}\mathbf{V}^H \tag{20}$$

with $\mathbf{S} = diag(s_j)$, $j = 1, ..., 7N$ being the diagonal matrix containing the singular values, and hence $s_{7N} = 0$. The matrices $\mathbf{W}$ and $\mathbf{V}$ are orthonormal and the vector $\mathbf{Q}$ satisfying $\mathbf{Q}^H(i\omega_c\hat{\mathbf{G}} + \hat{\mathbf{L}}) = 0$ is given by the last column of $\mathbf{W}$. In Appendix A a discussion of the convergence properties of the eigensolutions $\hat{\mathbf{\Psi}}$ in (18) and the coefficients α_1, α_2 in (16a) for the standard parameter values is provided. The results presented below were obtained with $N = 35$, which guarantees sufficiently accurate solutions.

3 Results

3.1 Linear stability Analysis

We investigate the linear stability of system (2) along the path in parameter space that is shown in Fig. 1. The locations indicated with $\mathbf{K}$ $((\delta_{sst}, \kappa_z, kTh) = (0,0,1))$ and $\mathbf{R}$ $((\delta_{sst}, \kappa_z, \kappa_{Th}) = (1, \kappa_z, 0))$ correspond to reductions of the SST equation to Model I and Model IV of Hirst (1986). The standard values of the parameters correspond to the case labeled with M in Fig. 1 and are at $\kappa_z = -0.01$ and $\kappa_{Th} = 0.15$. For these conditions the neutral curve, separating regions of growth from decay in parameter space, is plotted as

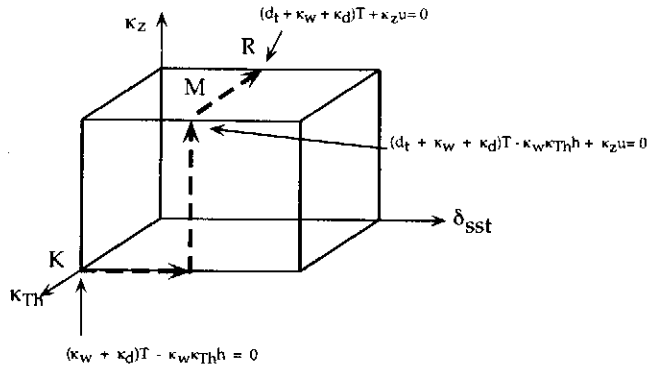

Fig. 1. The path in parameter space along which the calculations have been performed. The governing sea surface temperature equation is shown for each regime.

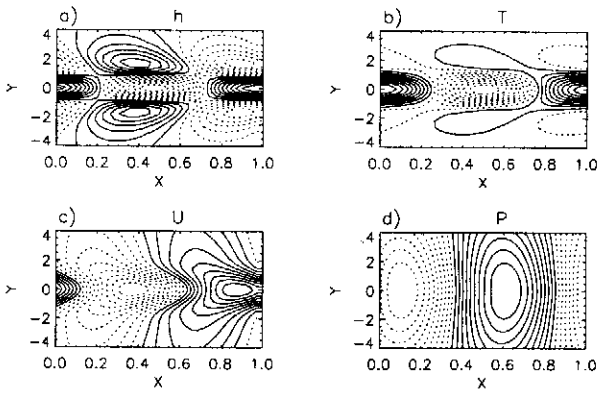

Fig. 3. The eigenvectors of the most unstable wave, corresponding to the minimum of the neutral curve of Fig. 2.
The eigenvectors of the most unstable wave, corresponding to the minimum of the neutral curve of Fig. 1 . (a) Thermocline depth, (b) sea surface temperature; the drawn (dotted) contours indicate positive (negative) anomalies.(c) Zonal atmospheric surface wind anomaly, the drawn (dotted) contours indicate eastward (westward) winds. (d) Low level pressure anomaly, the drawn (dotted) contours indicate high (low) pressure.

a function of the wavenumber k and the coupling parameter μ in Fig. 2. Since this neutral curve has a minimum at $k_c = 0.11, \mu_c = 1675$, it allows one to identify the dominant mode in the system, i.e. the first mode to become unstable when the coupling strength is increased. The patterns of thermocline depth , SST, zonal surface wind and atmospheric pressure perturbations of the dominant mode just at criticality are shown in Figs. 3. These spatial patterns show the mixture of Kelvin, Rossby and SST mode character.

The critical point is followed along the path in Fig. 1 and is plotted in the plane of wavenumber k and coupling strength μ in Fig. 4a. The wavelength of the dominant mode increases from 7300 km for the coupled Kelvin mode to 15.000 km for the coupled Rossby mode. In Fig. 4b the growth rates of the two most unstable modes are plotted along the same path. The dominant mode has zero growth rate, the second is damped. Clearly, there is only one mode which is deformed in a continuous way from a coupled Kelvin mode via a mixed SST-mode into a destabilized coupled Rossby mode. This is confirmed by the phase - and group velocities of the first mode as shown in Fig. 4c. Here negative values of the phase ω indicate eastward propagation. The dominant period of the

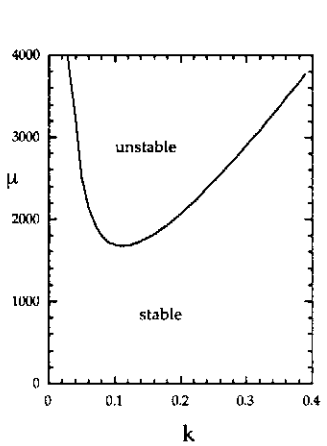

Fig. 2. The neutral curve of wavenumber versus coupling strength $(\delta_{sst}, \kappa_z, \kappa_{Th}) = (1, -0.01, 0.15)$ and the parameter values as in Table 2.

critical mode increases slowly from 90 days (dimensional period is $\frac{2\pi}{\omega}\mathcal{T}_o$) for the Kelvin mode to a standing wave as advection is balanced by upwelling feedback. In the advective regime a 120 day period westward traveling coupled Rossby wave is found. The energy of all the coupled instabilities travels eastward, as is indicated by the sign of the groupvelocity c_g (Fig. 4c).

The picture of one coupled mode which changes character when parameters are varied, and where different instability mechanisms dominate the growth is in agreement with the continuous connection of eigensurfaces in the ocean basin case, as was shown in Jin and Neelin (1993). It puts the results of Hirst (1986), where it seems as if essentially different modes are destabilized for different SST-equations, in a much simpler perspective. It is also found to be robust against variation of the other system parameters such as the atmospheric damping strength and the Kelvin wave speed ratio (c_a/c_o).

3.2 Weakly nonlinear stability analysis

The results of the linear theory of the previous section provide the basis to investigate the effects of different nonlinear interaction mechanisms to equilibrate the exponentially growing instabilities. If the initially unstable modes equilibrate on a $\mathcal{O}(1/\epsilon^2)$ time scale, these nonlinear effects determine both the amplitude and period of the finite amplitude traveling wave. The three different types of nonlinearities considered are (A) only nonlinear thermocline feedback, (B) both nonlinear thermocline feedback and advection in the SST equation and the full model (C) which also includes nonlinear ocean dynamics.

The nonlinear analysis is carried out along the path of Fig. 1 and the coefficients of the resulting Ginzburg-Landau

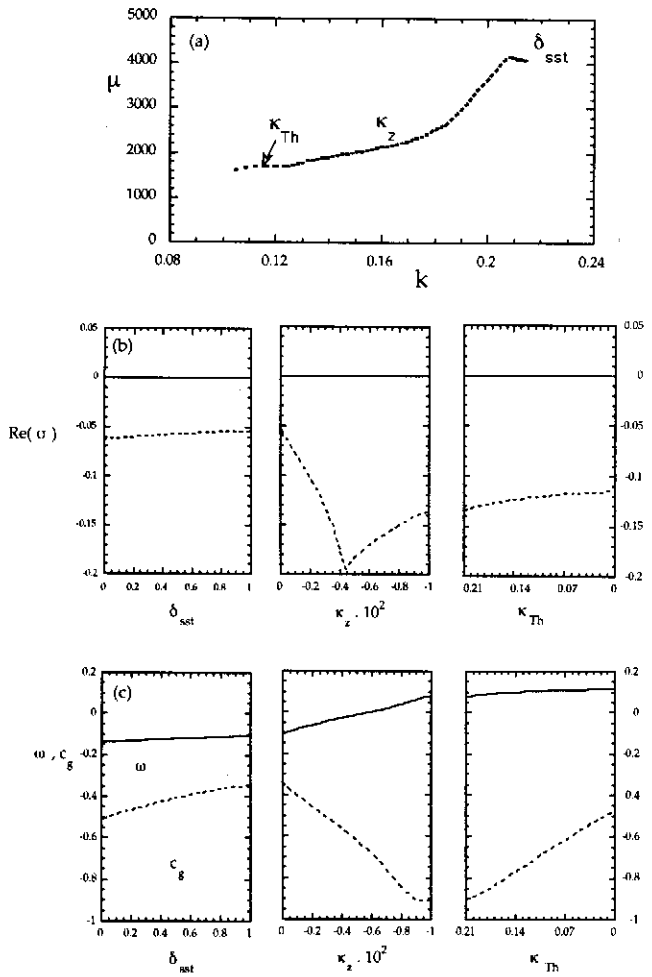

Fig. 4. (a) The position of the critical point on the neutral curve in the (k, μ)-plane as a function of $(\delta_{sst}, \kappa_z, \kappa_{Th})$. The arrow denotes the position of the critical point in Fig. 2
(b) The growth rates of the two least stable modes along the path of Fig. 1. The dominant mode has a zero growth rate and appears as a straight line.
(c) The frequency and group velocity of the critical mode along path of Fig. 1. Negative (positive) phase speeds (group velocities) indicate eastward (westward) traveling waves (energies).

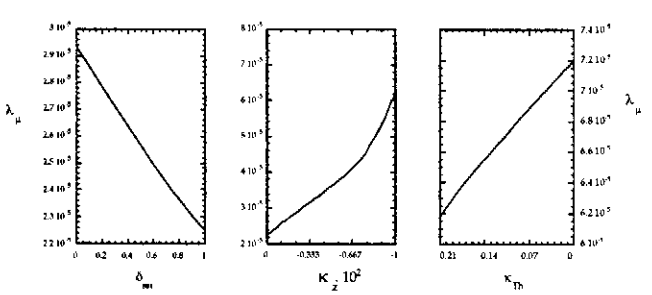

Fig. 5. The correction to the growth rate at neutral conditions along the path of Fig. 1. Note that the vertical scale differs for each panel.

are calculated along this path in parameter space. From a physical point of view, solutions to the Ginzburg-Landau equation describe the modulation of instablities in both time and space. In the previous section we have considered instabilities with wavelengths in the order of the Pacific zonal basin size. This implies that there will be no wavenumbers available for spatial modulation, without taking into account the effects of reflections at the meridional boundaries. This is beyond the scope of the reduced model presented here. Therefore, the term in (14a) associated with the spatial modulation, A_{XX}, will be neglected from now on. It turns out that for the parameter regimes considered, where the scaling (15) is valid, the Stokes wave solution given by

$$a(\tau) = e^{-i\alpha_2 \tau} \tag{21}$$

is stable solution. Physically, this solution introduces a frequency modulation of the most unstable mode in the zonally unbounded domain, whereas the amplitude is stationary. There are three important scales associated with finite amplitude equilibration. The e-folding time of the linear unstable mode sets the time scale of growth to finite amplitude and is given by (16d) :

$$t_e^* = \frac{1}{(\mu - \mu_c)\lambda_\mu} \mathcal{T}_o \tag{22a}$$

For each of the cases A-C this time scale is the same, since the underlying linear stability problem is identical. The factor λ_μ controls this growth, given the distance beyond criticality. In Fig.5 this factor is plotted and it is small because it is relative to the coupling strength μ_c which, as can be seen in Fig.4a, is large. As a measure of the strength at finite amplitude of the coupled anomaly in the system for each nonlinear scenario the dimensional value of SST at the equator is taken.

$$T^* = \sqrt{-(\mu - \mu_c)\frac{\lambda_\mu}{\Lambda_\tau}}\, \Delta T\, \hat{T}(0) \tag{22b}$$

Whereas the time scale of reaching finite amplitude is set by the linear theory, the amplitude itself is set by $-\Lambda_\tau$. Hence, if this quantity turns out to be positive, solutions on the equilibration time scale $\mathcal{O}(1/\epsilon^2)$ assumed in the weakly nonlinear theory, are not valid. In the latter case, finite amplitude equilibration occurs on a longer time scale. For fixed λ_μ, the magnitude of $-\Lambda_\tau$ measures the strength of the nonlinear interactions and the final amplitude. A large (small) value of $-\Lambda_\tau$ indicates strong (weak) interactions and a small (large) final finite amplitude. Obviously, for fixed $-\Lambda_\tau$, the instabilities grow faster (slower) with large (small) values of λ_μ and a larger (smaller) amplitude is reached.

In Fig. 6 the real and imaginary parts of Λ have been plotted for the cases A, B and C respectively along the path in Fig. 1. The nonlinear thermocline feedback is able to balance nearly all unstable modes along the path, except a small interval within panel 2 (Fig. 6a). Apparently, the westward propagation tendencies introduced by the zonal advection feedback are more difficult to balance by the thermocline feedback. The nonlinear zonal advection feedback widens the

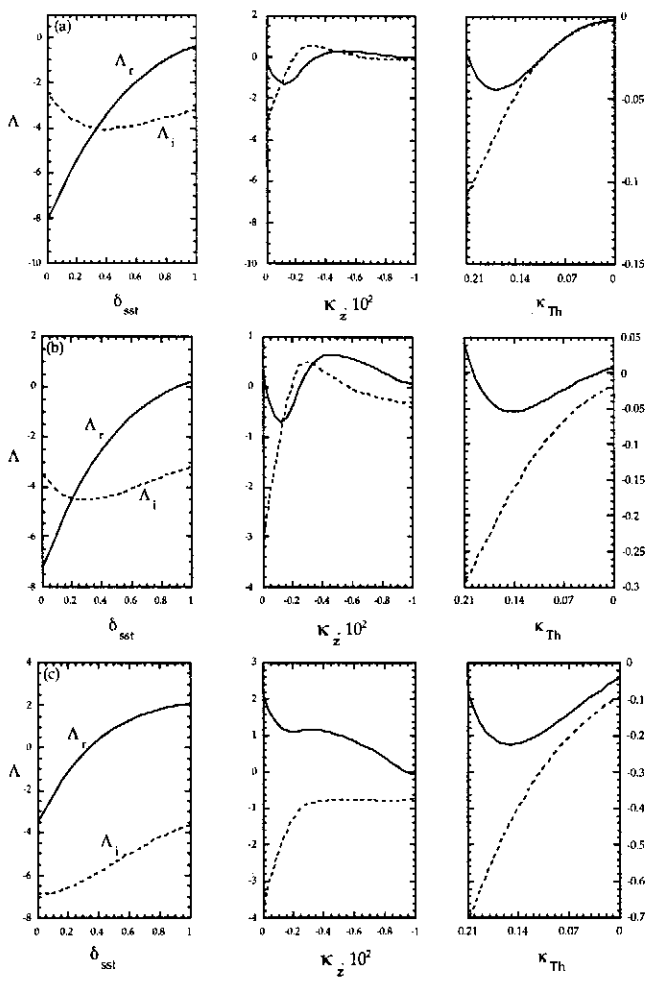

Fig. 6. The real and imaginary part of the Landau coefficient Λ of the critical mode along the path of Fig. 1 for the different nonlinear interactions considered in the model.
a) case A: only nonlinear thermocline feedback.
b) case B: nonlinear thermocline feedback and advection of SST.
c) case C: in addition to b) also nonlinear ocean dynamics.

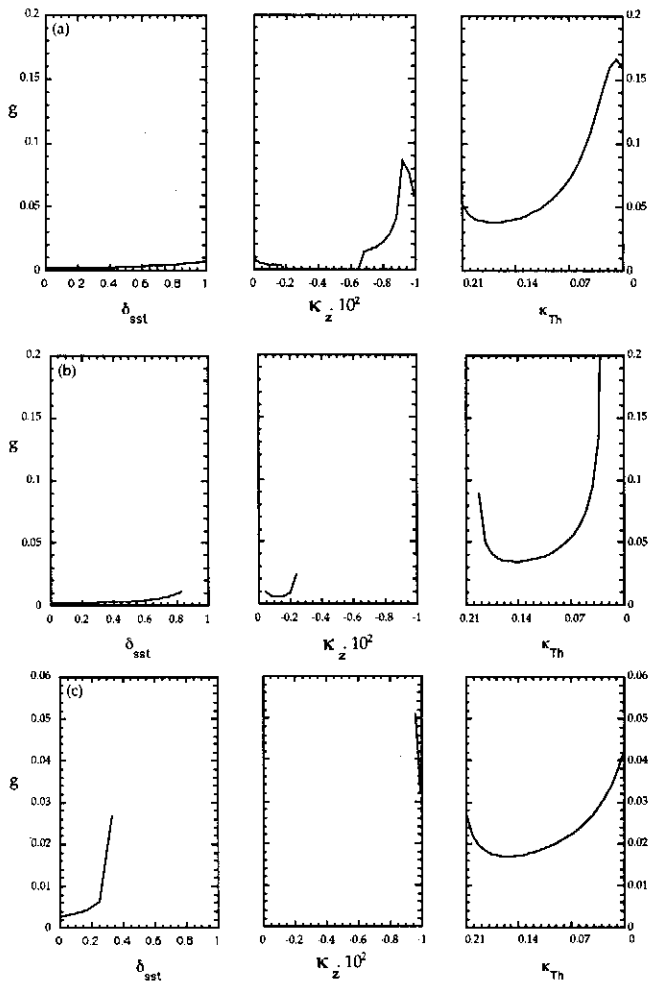

Fig. 7. The finite amplitude g of the initially unstable mode along the path of Fig. 1 for the nonlinear interactions considered in the model. The regions in parameter space where equilibration occurs are separated by asymptotes.
a) case A: only nonlinear thermocline feedback.
b) case B: nonlinear thermocline feedback and advection of SST.
c) case C: in addition to b) also nonlinear ocean dynamics.

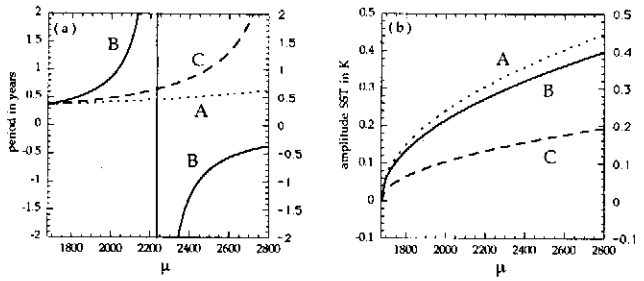

Fig. 8. The period (a) and the amplitude (b) of the stable limit cycle as a function of the distance from the critical conditions in Fig. 2, for the three nonlinear equilibration mechanisms.

regions where equilibration at the assumed time scale is not possible (Fig. 6b). The intervals over which Λ_r is positive become larger which indicates that the nonlinear interactions of advection and thermocline feedback cancel each other resulting in a net weaker interaction. This weakening is stronger when the instability is westward propagating. When nonlinear ocean dynamics is included, this weakening is seen, in Fig. 6c, for eastward propagating instabilities, but a strengthening results for westward propagating instabilities which are consequently more easily balanced. The Figs. 7 show the finite amplitude $g = \sqrt{\frac{-\lambda_\mu}{\Lambda_r}}$ for the cases A, B and C respectively along the path in Fig. 1. The regions of validity of the weakly nonlinear theory (where $\Lambda_r < 0$) are separated by asymptotes in the amplitude g. For the westward propagating disturbances, the amplitude is systematically larger due to the larger value of λ_μ and the smaller value of $-\Lambda_r$.

The period of the stable limit cycle attained by the linear instabilities is a third measure for comparing the effects of the different nonlinear interactions. This period is in dimensional units defined as

$$p_s^* = \frac{2\pi}{\omega_c + (\mu - \mu_c)(\omega_\mu - \lambda_\mu \alpha_2)} \mathcal{T}_0 \qquad (22c)$$

In this expression ω_c is the frequency of the linear unstable mode at critical conditions and ω_μ is its linear correction above criticality. For the standard parameter values corresponding to the neutral curve of Fig. 2 (and the patterns of the coupled mode in Fig. 3), the periods (Fig. 8a) and the finite amplitudes (Fig. 8b) for each of the three cases A, B and C, are plotted as a function of $\mu - \mu_c$.

As can be seen from the expression for p_s^*, the actual period induced at finite amplitude may depend strongly on the particular nonlinear interaction through the coefficient α_2. In case (A), the period of 4 months set by linear theory grows slowly to 8 months as μ is increased from critical conditions to a value of 2800. The amplitude of the SST-perturbations at the equator approaches 0.5 K. The addition of advection of SST-perturbations (case B) shows a dramatic impact on the period of the limit cycle. The initial period of the westward propagating instability increases through several years to a steady state near $\mu = 2300$. For even larger values of μ the propagation changes from westward to eastward. Nonlinear ocean dynamics generate stronger interactions resulting in a significantly smaller amplitude of the perturbations. The period of the oscillation responds much slower to increases in μ.

4 Low frequency time-dependent forcing

In the previous section, we have shown that the computation of finite amplitude traveling waves of the fully coupled model was reduced to the computation of coefficients of the Ginzburg- Landau equation. Amplitude and period then followed from properties of the Stokes wave. It was found that the typical time scales of instability were in the order of months. In this section, we study the possibility of deriving reduced models in case a time-dependent external forcing is present, for example the seasonal forcing on a time scale of about one year. In this case, the period of the external forcing is longer than that of the instabilities and one might ask how the finite amplitude equilibration of the perturbations, during their growth, alters due to the modifications of such an external influence. It turns out that under a certain scaling of the external forcing, as shown below, a similar reduced model can be derived.

4.1 Derivation of the reduced model

In the case under study, we imagine a time-dependent external forcing, for example in the zonal wind stress, which is zonally constant and has a prescribed meridional and temporal structure. The amplitude (and frequency) of this external wind field is small and scaled in such a way that it does not influence the linear stability properties, since the mean state remains the same. However, the response of this wind field may interfere with the growth of the disturbances. The strength of the external forcing has the same order of magnitude as modifications to the basic state due to nonlinear self-interactions of the perturbations. In this way, this correction to the basic state at $\mathcal{O}(\epsilon^2)$ becomes time-dependent and has its impact on the equilibration of the instabilities.

Hence, consider the general system (2) extended to include a small amplitude forcing term, i.e.

$$\begin{cases} (\mathcal{M}\frac{\partial}{\partial t} + \mathcal{L})\mathbf{\Phi} + \mathcal{N}(\mathbf{\Phi})\mathbf{\Phi} = \epsilon^2 \mathbf{F}(y, \nu\epsilon^2 t) \\ \mathcal{B}(\mathbf{\Phi}, y = \pm\infty) = \mathbf{0} \end{cases} \qquad (23)$$

The vector function $\mathbf{F}$ in the right hand side contains the forcing terms. After scaling of the system they appear to be small with respect to the terms on the left. This is expressed in the fact that the amplitude $\epsilon^2 \ll 1$, $\mathbf{F} = \mathcal{O}(1)$ and has no x- dependence. The scaling implies that the forcing acts on the long time scale similar to that of the equilibration of the instability in the unforced system. Consequently, it does not change the initial mechanism of growth of the instability. The forcing frequency ν is $\mathcal{O}(1)$ and the derivation of the amplitude equation is analogous to section 2a, except now the forcing term enters at $\mathcal{O}(\epsilon^2)$. If the forcing function has

the following structure

$$\mathbf{F}(y, \nu\epsilon^2 t) = \hat{\mathbf{F}}(y) f(\nu T) \tag{24}$$

the solution $\mathbf{\Phi}^{(02)}$ can be decomposed into

$$\mathbf{\Phi}^{(02)} = |A(X,T)|^2 \mathbf{\Psi}^{(02)} + \mathbf{\Psi}^F f(\nu T) \tag{25a}$$

where we retain the part consisting of the nonlinear self-interaction (cf. equation (10b))

$$\hat{\mathcal{L}}(0)\mathbf{\Psi}^{(02)} = -2Re(\mathcal{N}(\mathbf{\Psi})\mathbf{\Psi}^*) \tag{25b}$$

and a part caused by the external forcing

$$\hat{\mathcal{L}}(0)\mathbf{\Psi}^F = \hat{\mathbf{F}}(y) \tag{25c}$$

Since the operator $\hat{\mathcal{L}}(0)$ is invertible, both contributions to the solutions at $\mathcal{O}(\epsilon^2)$ are unique. Following the approach of section 2 one finds at $\mathcal{O}(\epsilon^3 E)$

$$(i\omega_c \hat{\mathcal{M}}(k_c) + \hat{\mathcal{L}}(k_c))\mathbf{\Phi}^{(13)} =$$

$$-(\hat{\mathcal{M}}(k_c)\mathbf{\Psi}\,\frac{\partial A}{\partial T} + \tilde{\mathbf{\Gamma}} A + \mathbf{\Sigma}\,\frac{\partial^2 A}{\partial X^2} + \mathbf{\Lambda}\, A|A|^2) \tag{26a}$$

where

$$\tilde{\mathbf{\Gamma}} = m\mathbf{\Gamma} - \mathbf{C} f(\nu T) \tag{26b}$$

with $\mathbf{\Gamma}$, $\mathbf{\Sigma}$ and $\mathbf{\Lambda}$ as in (13) and

$$\mathbf{C} = \mathcal{N}(\mathbf{\Psi}^F)\mathbf{\Psi} + \mathcal{N}(\mathbf{\Psi})\mathbf{\Psi}^F \tag{26c}$$

Note that if $f = 0$, the equations (26) reduce to those in (12). Application of the Fredholm alternative to (26a) results in a modified Ginzburg-Landau equation

$$\frac{\partial A}{\partial T} = \tilde{\gamma_1}(T) A + \gamma_2 \frac{\partial^2 A}{\partial X^2} - \gamma_3 |A|^2 \tag{27a}$$

where the, now time dependent, coefficient $\tilde{\gamma_1}$ is defined as

$$\tilde{\gamma_1} = \gamma_1 - c f(\nu T) \tag{27b}$$

with

$$c = c_r + i c_i = \frac{\mathbf{Q}^H \mathbf{C}}{\mathbf{Q}^H \hat{\mathcal{M}} \mathbf{\Psi}}, \tag{27c}$$

while the other coefficients γ_j are identical to those in (14). Writing in general

$$f(\nu T) = \delta + h(\nu T)$$

where h is now a $2\pi/\nu$-periodic function with zero mean and δ a constant, eq. (27a) can be written as

$$\frac{\partial a}{\partial \tau} = (1 - \alpha_0 h(\beta_0 \tau)) a + (1 + i\alpha_1)\frac{\partial^2 a}{\partial \xi^2} - (1 + i\alpha_2) a|a|^2 \tag{28a}$$

where time and amplitude have been rescaled according to

$$\tau = (m\lambda_\mu - \delta c_r) T\,,$$

$$a(\xi, \tau) = g^{-1} A(T, X) exp(-im\omega_\mu T + i\frac{c_i}{\nu} F(\nu T)) \tag{28b}$$

The amplitude g is now given by

$$g = \sqrt{\frac{m\lambda_\mu - \delta c_r}{-\Lambda_r}}, \tag{28c),}$$

and the real coefficients α_0, β_0 in (28a) are defined as $\alpha_0 = \frac{c_r}{m\lambda_\mu - \delta c_r}$ and $\beta_0 = \frac{\nu}{m\lambda_\mu - c_r \delta}$. The function $F(\nu T)$ appearing in (28b) is the primitive function of the function f. The amplitude equation (28a) reflects the equilibration of the dominant mode at finite amplitude affected by the oscillating nature of the applied low frequency forcing. Compared to (16a), one observes that in (28a) the growth rate is influenced by the time-dependent forcing on a time scale τ, due to a modification of the basic state.

4.2 Results

For the forcing term $\hat{\mathbf{F}}$, the following structure is assumed

$$\hat{\mathbf{F}}(y) = \begin{pmatrix} \tau^x(y) & 0 & 0 & 0 & 0 & 0 & 0 \end{pmatrix}^T \tag{29a}$$

with

$$\tau^x(y) = e^{-\frac{1}{2}\alpha y^2}\ ,\ \alpha = \frac{1}{\sqrt{c}} \tag{29b}$$

We now study the response due to a special form of $h(\nu T) = sin(\nu T)$ and all three equilibration mechanisms balancing linear growth (case C in section 3). The spatial derivatives in the modified Ginzburg-Landau equation (27a) are dropped at this point in the analysis, for the same reasons as given in section 3.2 for the reduced model without time-dependent coefficients. We focus on the parameters for the Landau-equation for the same case as in Figs. 8 and $\mu = 2000$, the forcing period is chosen to be approximately one year ($\nu = 1.4$). The original instability has a period of about three months (Fig. 8a) at neutral conditions. Solutions of the modified Landau equation are presented in Figs. 9 for three values of the offset δ. The power spectra derived from the time series for each of these cases are shown in Fig. 10.

For $\delta = 0$, the time-series in Fig. 9a indicates that very low frequency variability appears due to the presence of the external forcing. Note that if $\nu = 0$, the amplitude would be purely periodic with a period determined as in Fig. 8a of about 0.5 year (for $\mu = 2000$). The spectrum in Fig. 10 shows that indeed higher as well as lower frequency variability is introduced in the response. When the offset δ is positive (negative), this shifts the peaks in the spectrum to lower (higher) frequency and slightly decreases (increases) the amplitude. The latter is easily observed from the expression for g (in (28c)) because $c_r > 0$. The wind forcing has a fixed meridional structure and varies on a time scale of a year with a small amplitude. Although the instabilities would develop to limit cycles with a period of about half a year in the absence of this external forcing, the interaction of the nonlinear equilibration of the instabilities and simultaneous response to the external forcing give rise to very low frequency variability. To understand how this response is generated, closed

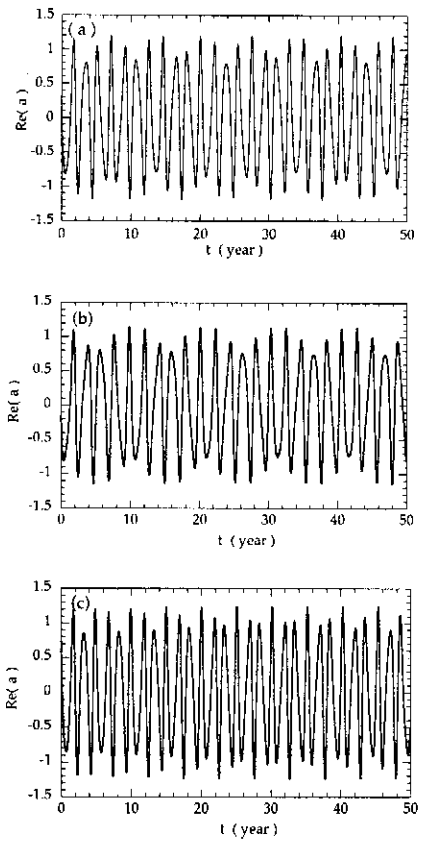

Fig. 9. Time series of a solution of the forced Landau equation for $\nu = 1.4$, corresponding to a forcing period of about 1 year. (a) $\delta = 0$. (b) $\delta = 0.2$. (c) $\delta = -0.2$. (d) Power spectra of the time series in a-c.

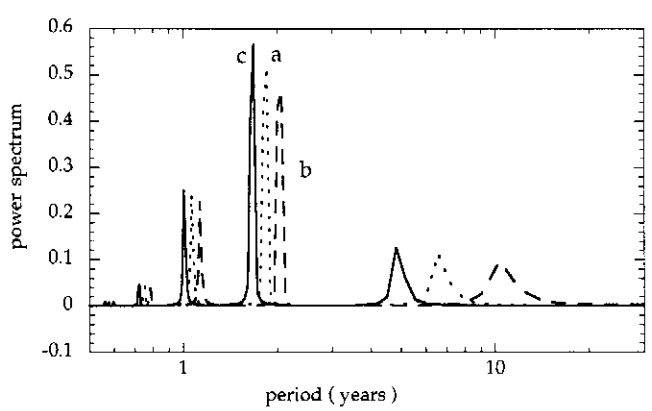

Fig. 10. Powerspectra of the timeseries of the solutions to the forced Landau equation shown in Fig. 9. (a) $\delta = 0$, (b) $\delta = 0.2$ and (c) $\delta = -0.2$.

form solutions to (28a) of the form

$$a(\tau) = R(\tau)e^{i\phi(\tau)} \tag{30}$$

are obtained in appendix B. It is shown that the phase $\phi(\tau)$ can be written as a sum of a linear function of τ and a periodic function of τ (the function $P_2(\tau)$ in appendix B). It is easily demonstrated that this periodic contribution to the phase is responsible for for the energy transfer towards lower frequencies as observed in Fig. 10. A simple example to consider is that $P_2(\tau) = sin(\frac{\pi}{2}\tau)$ in which case the amplitude a would oscillate as $sin(\tau + sin(\frac{\pi}{2}\tau))$, which obviously gives a low frequency signal. Hence, the periodic nature of the external forcing alone is able to induce much lower frequency behavior of the finite amplitude instabilities than would occur without it.

5 Summary and conclusions

The weakly nonlinear evolution of equatorial coupled ocean-atmosphere instabilities was considered in this paper. The basis for the nonlinear analysis are the Hirst (1986) coupled instabilities of a simple basic state within a model having a periodic ocean basin. The results found by Hirst (1986) suggest that for different limits of the SST-equation different waves become unstable related to dynamical modes of the uncoupled ocean/SST spectrum. Here we have connected these limits of the sea surface temperature equation, by varying its key parameters and calculating the dominant unstable mode along this path in parameter space. We found that there is only one mode dominating the dynamics, i.e. between the distinct regimes of SST-dynamics no exchange of stability occurs.

Our approach implies an extension of the Hirst (1986)-model to include nonlinear terms in both the ocean component and the SST-equation. This involved the derivation of a (Ginzburg-) Landau equation which describes the evolution of slightly unstable modes. Three different types of nonlinearities were considered to equilibrate the instabilities: nonlinear upwelling feedback in the SST-equation (case A), nonlinear advection of SST (case B) and nonlinear ocean dynamics (case C). In all three cases there exist regimes where finite amplitude equilibration is possible on a $\mathcal{O}(1/\epsilon^2)$ time scale, where ϵ measures the relative distance from criticality.

Over a range of parameters, eastward coupled Kelvin modes can become unstable due to coupled feedbacks inducing spatial patterns and frequencies similar to those in observations of intraseasonal variability in the equatorial Pacific. The subsequent equilibration can lead to considerable amplitudes of the deviations from the mean state, having a square root dependence on the distance from the onset of instability. The period of oscillation corresponding to the stable limit cycle was found to be increasing with coupling strength. The strength of each nonlinearity is completely measured by the value of the real part of the nonlinear coefficient $-\Lambda$ in the Ginzburg-Landau equation. For the same growth rate of the instability, a stronger nonlinearity will

finally induce a smaller finite amplitude. Apart from the methodology, which has a large application potential, the results for the periodic basin indicate that coupled processes in the ocean-atmosphere may substantially contribute to the intraseasonal variability in the equatorial Pacific.

The weakly nonlinear analysis also allowed for the study of the effect of annual frequency external forcing on the evolution of the unstable modes. Assuming that this forcing has a small amplitude, a modified Ginzburg-Landau equation can be derived to describe the equilibration of the instabilities. The analysis of its solutions for the case of a slowly varying external wind stress reveals that the forcing introduces interannual variability due to the periodic nature of the phase correction. The reduced model is attractive because the interactions between nonlinear equilibration and low frequency external forcing can be analyzed in considerable detail. In particular, the interannual frequency response is shown to be generated because the growth rate contains a periodic component, which induces a periodic correction in the phase of the solution for the amplitude. The results are suggesting that unstable air-sea interactions, through intraseasonal waves and weak external annual forcing are able to influence the development of ENSO events although the exact connection obviously requires further study.

Appendix A. Convergence properties

The orthogonal basis of rational Chebychev polynomials introduces, due to the meridional unboundedness of the equatorial β-plane an extra parameter L. Since both the ocean as well as the atmosphere have different Rossby deformation radii, one would like to expand variables of both components of the system in basisfunctions that inhibit these natural scales. However, comparisons of solutions obtained for different values of L for ocean and and for the atmosphere variables indicate poor convergence properties with the number of polynomials. For this case, it was found that although the actual eigenvectors $\mathbf{\Psi}$ in (18) showed exponential decay in their spectral coefficients, the adjoint vector $\mathbf{Q}^H$ did not show any sign of convergence. This results in poor convergence properties for the coefficients of the Ginzburg-Landau equation.

Therefore the calculations presented here were done for $L = 3$ for both ocean and atmosphere. The solutions were not very sensitive to larger values of L. The numerical code used has been validated against the linear stability results in Hirst (1986). Furthermore the results have been checked against a discretization using a basis of Hermite functions. In Fig. A1, the convergence of the critical wavenumber k_c and the coefficient α_2 in ((16a) is shown as a function of the number of rational Chebychev modes (N) for $L = 3$. All calculations presented in this paper were done for $N = 35$. Although $N = 20$ is sufficient to solve the linear stability problem accurately enough, this number of modes is necessary to obtain sufficient accuracy in the coefficient α_2.

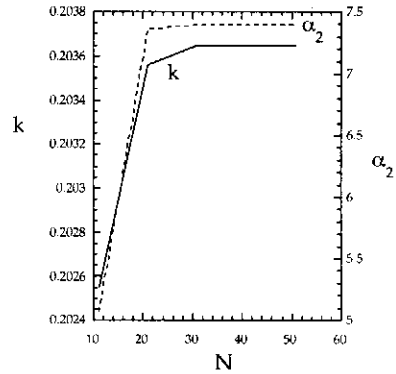

Fig. A1. The convergence of the wavenumber k at a critical point and the nonlinear coefficient of the (Ginzburg-) Landau equation as a function of the number of Chebychev modes N.

Appendix B. Solutions to the forced Landau equation

The forced Landau equation reads

$$\frac{\partial a}{\partial \tau} = (1 - \alpha_0 h(\beta_0 \tau))a + (1 + i\alpha_1)\frac{\partial^2 a}{\partial \xi^2} - (1 + i\alpha_2)a|a|^2 \qquad (B.1)$$

Solutions, lacking ξ-dependence, of the form

$$a(\tau) = R(\tau)e^{i\phi(\tau)} \qquad (B.2)$$

with r and ϕ real functions of τ, are sought. Substitution into (B.1) and separating the real and imaginary parts yields

$$\frac{dR}{d\tau} = (1 - \alpha_0 h(\beta_0 \tau))R - R^3 \qquad (B.3a)$$

$$\frac{d\phi}{d\tau} = -\alpha_2 R^2 \qquad (B.3b)$$

The frequency ϕ and the amplitude R are decoupled, resulting in an evolution equation for the amplitude, the frequency is slaved to R. Concentrating on the amplitude, we multiply (B.3a) with R and rescale time to obtain

$$\frac{dr}{ds} = (1 - \alpha_0 h(\frac{1}{2}\beta_0 s))r - r^2 \qquad (B.4)$$

with $s = 2\tau$ and $r = R^2$.

Solutions to (B.4) are written as

$$r(s) = \frac{d}{ds} log(f(s)) = \frac{f'(s)}{f(s)} \qquad (B.5a)$$

where $f'(s)$ is the derivative of $f(s)$ with respect to s. Substitution into (B.4) leads to the solution for $f(s)$.

$$f(s) = C_1\left(\int_0^s e^{s' - H(\frac{1}{2}\beta_0 s')} ds' + C_2\right) ,$$

$$H(\frac{1}{2}\beta_0 s) = \int_0^s \alpha_0 h(\frac{1}{2}\beta_0 z) dz \qquad (B.5b)$$

If the initial condition $r(\tau = 0) = r_0$ is prescribed, the constant C_2 must satisfy $C_2 = r_0 exp(H(0))$ (C_1 drops out of

the expression for $r(s)$). The periodic nature of the phase ϕ can be demonstrated by expressing $f'(s)$ in terms of a Fourier series, i.e.

$$f'(s) = e^{s+H(\frac{1}{2}\beta_0 s')} = e^s(k_0 + \sum_{n=1} k_n cos(\frac{1}{2}\beta_0 ns + \theta_n)) \quad (B.6a)$$

where k_n and θ_n are the appropriate Fourier coefficients of $exp(H(\frac{1}{2}\beta_0 s))$. Integration of (B.6a) yields

$$f(s) = e^s(k_0 + \sum_{n=1} q_n(cos(\frac{1}{2}\beta_0 ns + \theta_n)$$

$$+\frac{1}{2}\beta_0 nsin(\frac{1}{2}\beta_0 ns + \theta_n)) + C_2 e^{-s}), \quad (B.6b)$$

where $q_n = \frac{k_n}{1+(\beta_0 n/2)^2}$. For large s the solution for the amplitude r has the following form

$$r(s) = (k_0 + \sum_{n=1} k_n cos(\frac{1}{2}\beta_0 ns + \theta_n)) \quad \times$$

$$(k_0 + \sum_{n=1} q_n(cos(\frac{1}{2}\beta_0 ns + \theta_n) + \frac{1}{2}\beta_0 nsin(\frac{1}{2}\beta_0 ns + \theta_n)))^{-1}$$

Again, this expression, being a periodic function, is expressed as a Fourier series, yielding

$$r(s) = r_0 + P_1(\frac{\beta_0}{2}s) \quad (B.7b)$$

P_1 contains the periodic terms in the series expansion of $r(s)$. The frequency ϕ is found to be

$$\phi(s) = -\frac{1}{2}\alpha_2 r_0 s - \frac{1}{2}\alpha_2 P_2(\frac{1}{2}\beta_0 s) \quad (B.7b)$$

where P_2 is the integral of P_1, also periodic and demonstrates the periodic component of the phase ϕ. Returning to the original variables, starting with the expansion (8), the solution $\epsilon\Phi^{11}E$ for large $\epsilon^2 t$ now reads

$$\Phi(x,y,t) = \sqrt{\mu - \mu_c}\, g\, R(\epsilon^2 t) e^{ikx} e^{i\theta(t)}\, \hat{\Phi}(y) \quad (B.8a)$$

where the amplitude $R(\epsilon^2 t)$ and phase $\theta(t)$ are defined as

$$R(t) = \sqrt{r_0 + P_1(\nu\epsilon^2 t)} \quad (B.8b)$$

and

$$\theta(t) = [\omega_c + (\mu - \mu_c)(\omega_\mu - \lambda_\mu r_0 \alpha_2)]t - \epsilon^2\delta(c_i + c_r r_0 \alpha_2)t$$

$$+\frac{c_i}{\nu}H(\nu\epsilon^2 t) + \frac{1}{2}\alpha_2 P_2(\nu\epsilon^2 t) \quad (B.8c)$$

Acknowledgements. This work was supported by the Dutch National Research Programme on Global Air Pollution and Climate Change, through projects 853110 (NOP I) and 951235 (NOP II). All computations were performed on the CRAY C98 at the Academic Computing Centre (SARA), Amsterdam, the Netherlands within the project SC283. Use of these computing facilities was sponsored by the Stichting Nationale Supercomputer faciliteiten (National Computing Facilities Foundation, NCF) with financial support from the Nederlandse Organisatie voor Wetenschappelijk Onderzoek (Netherlands Organization for Scientific Research, NWO).

References

Bjerknes, J. P., Atmospheric teleconnections from the equatorial Pacific., *Mon. Wea. Review, 97*, 163–172, 1969.

Boyd, J. P., The nonlinear equatorial Kelvin wave., *J. Phys. Ocean., 10*, 1–11, 1980.

Boyd, J. P., Equatorial solitary waves. Part I: Rossby Solitons., *J. Phys. Ocean., 10*, 1699–1717, 1980.

Boyd, J. P., Spectral methods using rational basis functions on an infinite interval., *J. Comp. Physics, 69*, 112–142, 1987.

Chen, K. P. and Joseph, D. D., Application of the singular value decomposition to the numerical computation of the coefficients of amplitude equations and normal forms., *Appl. Num. Math., 6*, 425–430, 1990.

Enfield, D. B., The intraseasonal oscillation in the eastern Pacific sea levels: How is it forced ?, *J. Phys. Ocean., 17*, 1860–1876, 1987.

Gill, A. E., Some simple solutions for heat induced tropical circulation., *Quart. J. Roy. Meteor. Soc., 106*, 447–462, 1980.

Hirst, A. C., Unstable and damped equatorial modes in simple coupled ocean-atmosphere models., *J. Atm. Sc., 43*, 606–630, 1986.

Hirst, A. C. and Lau, K. M., Intraseasonal and interannual oscillations in coupled ocean-atmosphere models., *J. Clim., 3*, 713–715, 1990.

Jin, F. F. and Neelin, J. D., Modes of interannual tropical ocean-atmosphere interaction - a unified view. Part I: Numerical results., *J. Atm. Sc., 50*, 3477–3503, 1993.

Johnson, E. S. and McPhaden, M. J., Structure of intraseasonal Kelvin waves in the equatorial Pacific Ocean., *J. Phys. Ocean., 23*, 608– 625, 1993.

Kessler, W. S., M. M. J. and Weickmann, K. M., Forcing of intraseasonal Kelvin waves in the equatorial Pacific., *J. Geoph. Res., 100*, 10,613–10,631, 1995.

Lau, K. M. and Shen, S., On the dynamics of intraseasonal oscillations and ENSO., *J. Atm. Sc., 45*, 1781–1797, 1988.

McPhaden, M. J. and Taft, B. A., Dynamics of seasonal and intraseasonal variability in the eastern equatorial Pacific., *J. Phys. Ocean., 18*, 1713–1732, 1988.

Neelin, J. D., The slow sea surface temperature mode and the fast-wave limit: Analytic theory for tropical interannual oscillations and experiments in a hybrid coupled model., *J. Atm. Sc., 48*, 584–606, 1991.

Newell, A. C. and Whitehead, J. A., Finite bandwidth, finite amplitude convection., *J. Fluid Mech., 38*, 279–303, 1969.

Newell, A. C., Passot, T., and Souli, M., The phase diffusion and mean drift equations for convection at finite Rayleigh numbers in large containers., *J. Fluid Mech., 220*, 187–252, 1990.

Philander, S. G. H., *El Niño and the Southern Oscillation.*, Academic Press, New York, 1990.

Spillane, M. C., Enfield, D. B., and Allen, J. S., Intraseasonal oscillations in sea level along the west coast of the Americas, *J. Phys. Ocean., 17*, 313–325, 1987.

Wakata, Y. and Sarachik, E. S., Nonlinear effects in coupled atmosphere-ocean basin modes, *J. Atm. Sc., 51*, 909–920, 1994.

Zebiak, S. E. and Cane, M. A., A model El Niño-Southern Oscillation., *Monthly Weather Review, 115*, 2262–2278, 1987.